Real-Time *In Situ* Light Scattering and X-ray Scattering Studies of Polyethylene Blown Film Deformation

MICHAEL F. BUTLER,[1] ATHENE M. DONALD[2]

[1] Department of Materials Science and Metallurgy, University of Cambridge, New Museums Site, Pembroke Street, Cambridge CB2 3QZ, United Kingdom

[2] Department of Physics, Cavendish Laboratory, University of Cambridge, Madingley Road, Cambridge CB3 0HE, United Kingdom

Received 10 March 1997; accepted 6 June 1997

ABSTRACT: A series of linear low-density polyethylene blown films were studied using the techniques of time-resolved, small-angle X-ray scattering (SAXS) using a synchrotron source and a time-resolved, small-angle light scattering. Scattering patterns and the load-extension curve were obtained simultaneously during deformation. It was found that the initial orientation of the film, with respect to the tensile axis, was important in determining the operative elastic deformation modes. Films drawn parallel to the machine direction (MD) showed evidence for lamellar separation, whereas interlamellar shear occurred in films drawn parallel to the transverse direction. In films drawn at 45° to MD, lamellar stack rotation was observed *via* SAXS. In all cases, the yield point corresponded to the activation of crystallographic deformation and the onset of the disruption of crystalline lamellae. In films drawn parallel to MD, the SAXS showed a distinct 4-point pattern upon macroscopic yield, indicating lamellar corrugation. Regardless of the initial orientation, a fibrillar morphology was achieved at some strain after yield that coexisted with the fragmenting lamellar morphology. Comparison of results from deformed spherulitic bulk samples showed that the study of oriented blown film containing a stacked lamellar morphology may be used, to a first approximation, as a model for the deformation of different regions of spherulites in unoriented spherulitic samples. © 1998 John Wiley & Sons, Inc. J Appl Polym Sci **67:** 321–339, 1998

Key words: polyethylene; deformation; SAXS; SALS

INTRODUCTION

The production of blown film is a common industrial process, schematically illustrated in Figure 1, which results in preferred orientation. As the molten polymer is extruded upward through an annular die to form a film, orientation is produced in the hot, amorphous material by the action of a longitudinal velocity gradient. Air is introduced at the bottom of the die, thus inflating the tube of polymer and forming a bubble. An air ring is used to cool the hot bubble and solidify it at a point above the die exit (the frost line). The inflated solidified bubble is flattened as it passes through nip rollers, which also serve to provide the axial tension to draw the film upwards. The material crystallizes from the oriented melt, the morphology produced being affected by the temperature of the melt leaving the extruder, the ratio of the tube diameter to the die diameter, the upward film velocity, and the freeze line height. The direction in the plane of the film and parallel to the drawing direction is known as the machine direction (MD). Perpendicular to the MD and also in

Correspondence to: A. M. Donald.

Journal of Applied Polymer Science, Vol. 67, 321–339 (1998)
 CCC 0021-8995/98/020321-19

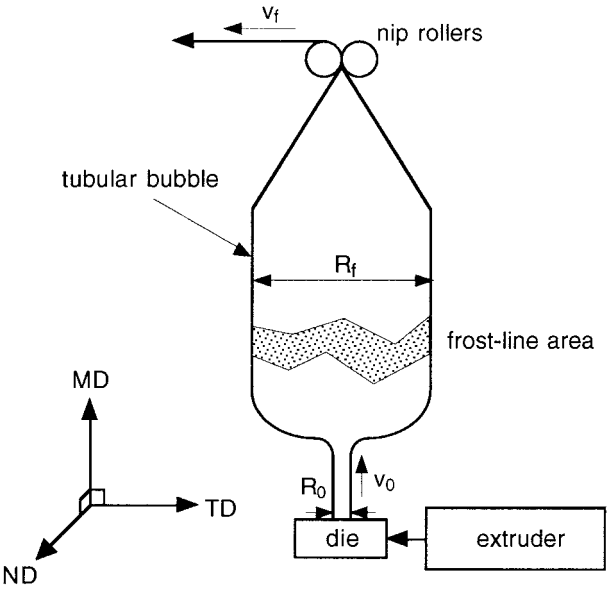

Figure 1 A schematic illustration of the blown film process.

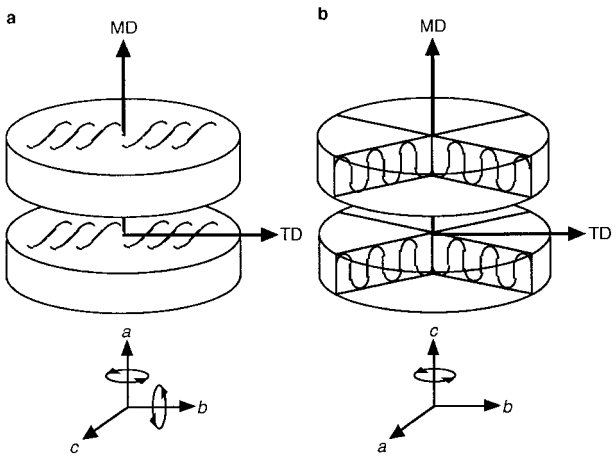

Figure 2 Morphologies produced by crystallization under stress: (a) Keller/Machin I morphology produced under low stress conditions; (b) Keller/Machin II morphology formed under high stress conditions.

the plane of the film is the transverse direction (TD). The normal direction is perpendicular to the TD and MD, being normal to the film surface.

Numerous studies have been performed using X-ray pole figure analysis,[1–7] small-angle X-ray scattering (SAXS),[4,8] light scattering,[9–11] electron microscopy,[10,12] infrared dichroism,[1,13] and birefringence measurements[1,6] to elucidate the morphology of blown film. It is generally accepted that the results describe a morphology consisting of rows of lamellae with their normals parallel to the extrusion (MD) direction. The lamellae frequently have the same width in each row, giving the appearance of nucleation from a central thread or fibrous core, possibly formed from extended chains, running parallel to the extrusion direction.[7,12] This morphology is known as a shish-kebab structure.[14] Whereas the existence of a central nucleus has been well substantiated in flow-induced solution crystallization,[15] it is still a matter of controversy for melt-crystallized blown films. A model for crystallization under stress has been described by Keller and Machin,[15] and has been used to account for the observed morphologies in polyethylene (PE) blown film.[7]

According to this model, two major types of crystallization take place, depending on the magnitude of the stress in the melt. Under low-stress conditions, the lamellae grow radially outward in the form of twisted ribbons, with their growth axis parallel to the *b* crystallographic axis for PE. This crystallization process causes a preferential orientation of the *a* axis parallel to the extrusion direction [Keller/Machin I morphology, shown in Fig. 2(a)]. Under higher stresses, the radially grown lamellae extend directly outward without twisting, causing the regularly folded chains within the lamellae (i.e., the crystallographic *c* axis) to remain parallel to the molecular chains in the extended microfibers [Keller/Machin II morphology, shown in Fig. 2(b)]. Intermediate stresses can, in theory, give a combination of the two morphologies. Whereas SAXS has verified the presence of row-nucleated lamellar stacks oriented parallel to MD,[8] wide-angle X-ray scattering (WAXS) pole figures have assessed the molecular orientation[7] and have distinguished between the two types of morphology.

Table I Information from DSC

Sample	Melting Temperature (°C)	Lamellar Thickness (nm)	Percentage Crystallinity
G	120.1 ± 1.0	10.8 ± 0.4	33.9 ± 1.9
	122.9 ± 0.2	12.2 ± 0.1	
H	125.2 ± 0.5	13.5 ± 0.2	38.7 ± 3.3
N	121.4 ± 0.1	11.4 ± 0.1	33.2 ± 1.0
	124.0 ± 0.2	12.8 ± 0.1	
O	109.6 ± 0.2	7.7 ± 0.1	33.8 ± 0.1
	116.4 ± 0.2	9.5 ± 0.1	
	121.3 ± 0.4	11.4 ± 0.2	
P	104.8 ± 2.3	6.8 ± 0.4	32.4 ± 1.1
	115.6 ± 0.2	9.2 ± 0.1	
	122.2 ± 0.3	11.8 ± 0.1	

The Keller/Machin I morphology is the most commonly observed morphology in PE blown films, with some reports of the combined intermediate morphology.[7] The Keller/Machin II morphology has only been induced in high-density polyethylene (HDPE) films, in which higher melt stresses are achieved.[7] Finally, it should be noted that a transcrystalline layer at the film surface has been identified in some blown film samples.[5,7] This layer arises because the film surface also acts as a site for heterogeneous nucleation. However, owing to the proximity of the nucleation sites, development of a spherulitic morphology is impeded, forcing the direction of lamellar growth parallel to the film normal. The thickness of the transcrystalline layer has some effect on the mechanical properties of the film,[1] becoming more detrimental with increasing layer thickness.

This article follows from a series of real-time X-ray scattering investigations[16,17] of unoriented PEs deformed in both tension and compression,

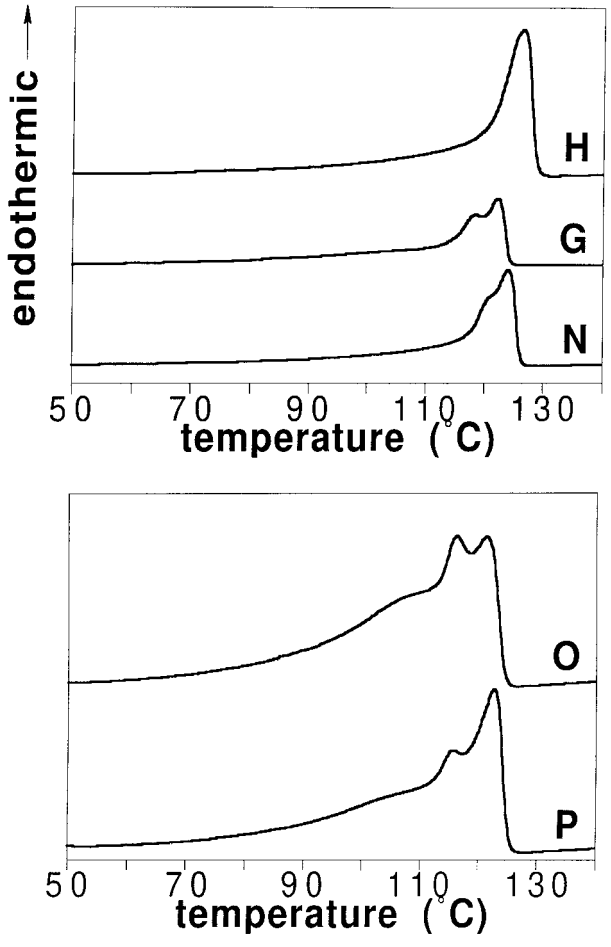

Figure 3 DSC traces from the undeformed blown films.

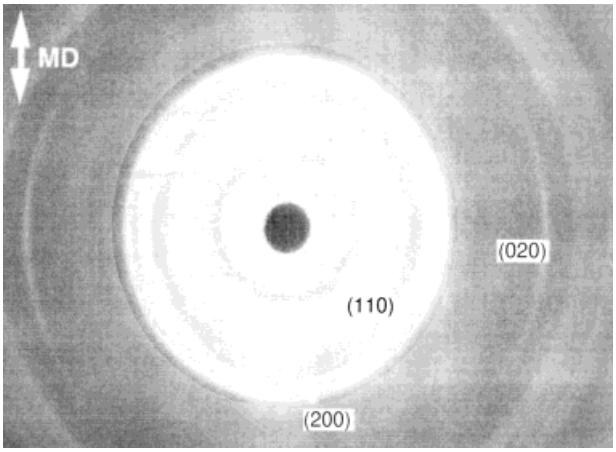

Figure 4 Two-dimensional image plate WAXS pattern from undeformed sample P.

and presents an investigation into the mechanical properties of linear low-density PE (LLDPE) blown film using synchrotron X-ray scattering (mainly SAXS) and small-angle light scattering (SALS) to probe the development of the microstructure in real-time during uniaxial tension at room temperature.

EXPERIMENTAL

Materials and Sample Characterization

A range of LLDPE blown films with different branch types [ethyl, butyl, isobutyl, and hexyl formed from the copolymerization of ethylene with butene (sample G); hexene (sample N); 4-methyl-1-pentene (sample H); and octene (samples O and P, respectively] were supplied by BP Chemicals Ltd (Sunbury, UK). Differential scanning calorimetry (DSC) was used to provide information on the lamellar thicknesses and percentage of crystallinities, as described previously.[16]

Separate specimens were cut from the blown film sheets with the MD parallel, perpendicular, and at 45° to the tensile axis, respectively. These specimens will hereafter be referred to as MD, TD, and 45, respectively.

X-ray Scattering

Two dimensional SAXS patterns were obtained during deformation using an electronic gas-filled multiwire area detector on beamline 16.1 at the Synchrotron Radiation Source (SRS) at Daresbury, UK. Details of this beamline and of the SRS have been given elsewhere.[18,19] Details

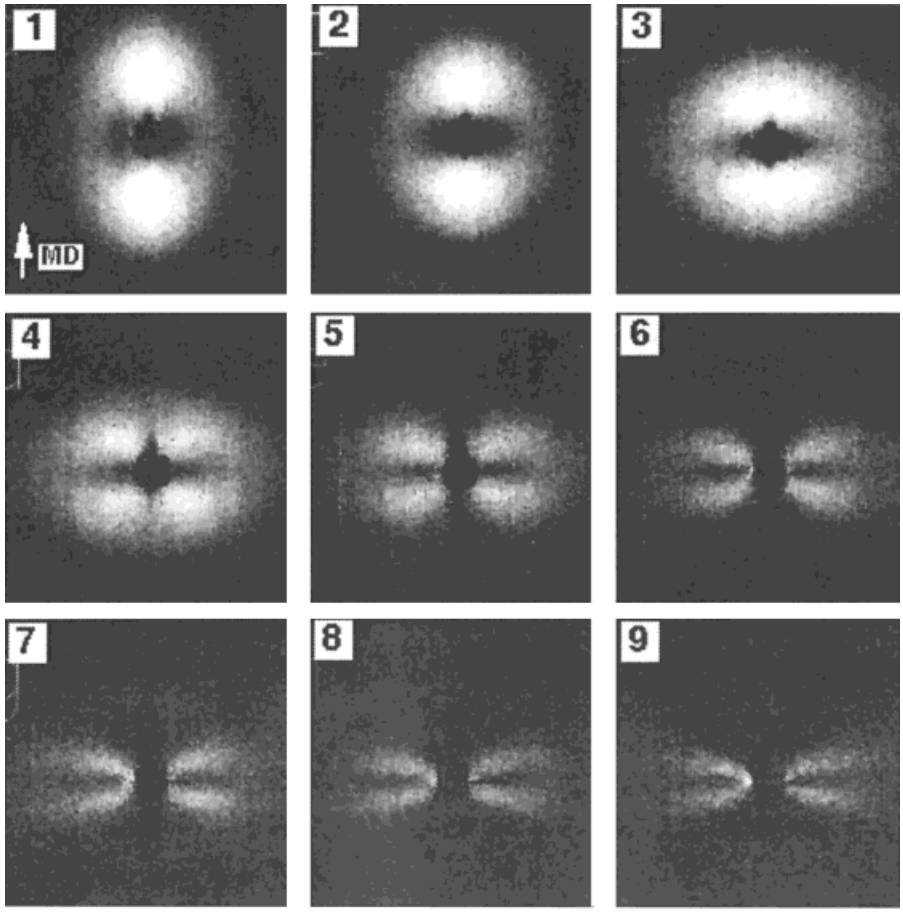

(a)

Figure 5 (a) Sequence of SAXS patterns and (b) the simultaneously obtained load-extension curve for sample P drawn parallel to MD (marked "MD"). The tensile axis and MD are vertical.

of the experimental set-up used at the SRS for simultaneously obtaining X-ray scattering patterns and the load-extensioncurve during deformation have been given in previous publications.[16,17] A SAXS pattern was obtained every 30 s during drawing to a final nominal strain of 570% at a nominal strain rate of $4.7 \times 10^{-3}\ s^{-1}$, at room temperature.

Two dimensional WAXS patterns were obtained on image plates from undeformed samples to characterize the crystalline orientation in the undeformed material.

SALS

SALS was used to investigate the deformation of the microstructure of samples G and H at length scales of $\sim 1\ \mu m$. The light scattering apparatus has been described in detail previously.[20]

Specimens, in the three orientations described earlier, were drawn at a nominal strain rate of $1.2 \times 10^{-3}\ s^{-1}$ to a final nominal strain of 430%. Two-dimensional SALS patterns were obtained every 10 s. The load-extension curve was simultaneously recorded. SALS patterns were obtained from (separate) samples in both H_v (between crossed polars) and V_v (polars uncrossed) configurations for the MD specimens and in the H_v configuration for the TD and 45 specimens.

RESULTS

Results from DSC are presented in Table I. Figure 3 displays the DSC traces for all of the samples, showing the lamellar thickness distribution to be trimodal for the hexyl-branched materials (shown by three distinct melting points), bimodal for the ethyl- and butyl-branched materials, and unimodal for the isobutyl-branched sample. The per-

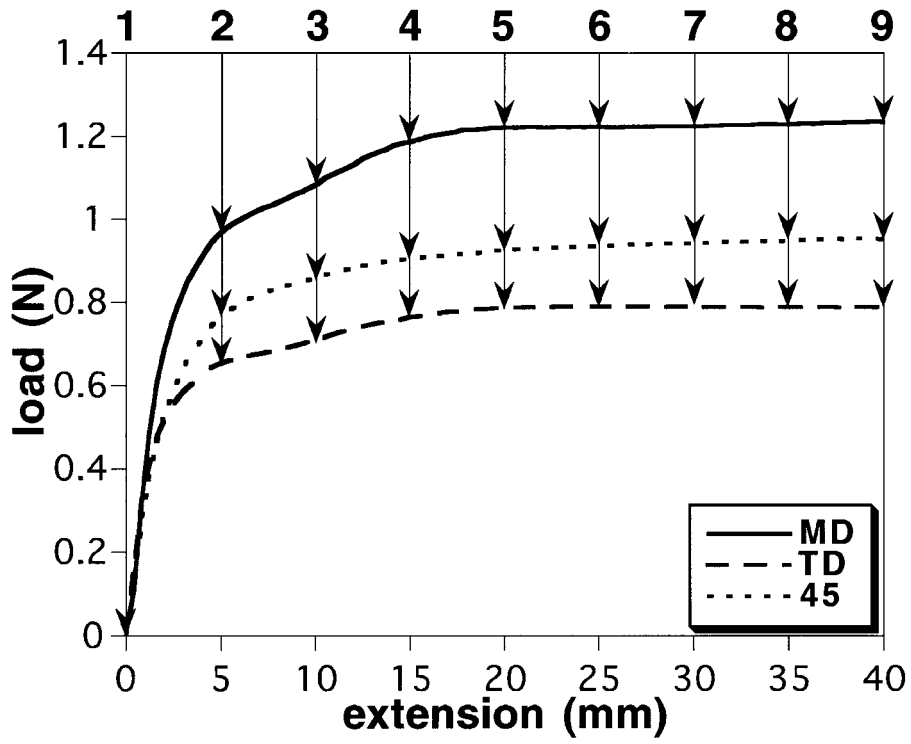

(b)

Figure 5 (*Continued from the previous page*)

centage of crystallinities was fairly similar, with the isobutyl-branched material possessing a slightly higher value, in accordance with the trend observed in unoriented samples of the same copolymers.[17]

WAXS

Figure 4 shows the WAXS pattern from one of the undeformed hexyl branched materials (P), which is representative of all of the samples. The pattern is typical of one from the Keller/Machin I morphology.

Time-Resolved SAXS

A two-spot SAXS pattern parallel to MD was obtained for all of the undeformed samples, indicating a stacked lamellar morphology with the lamellar normals parallel to MD. In addition, both hexyl-branched materials O and P exhibited a much weaker diffraction ring, indicating the presence of some unoriented lamellae in these samples. The hexyl-branched materials possessed the shortest long spacings. The isobutyl-branched sample possessed the largest long spacing, which again was consistent with the properties exhibited by bulk unoriented samples of the same materials.[17]

Drawing Parallel to MD

Figure 5 shows a sequence of SAXS patterns [Fig. 5(a)], together with the simultaneously obtained load extension curve for the hexyl-branched sample P drawn parallel to MD [Fig. 5(b)]. In Figure 6, the long spacings parallel and perpendicular to MD (L_{MD} and L_{TD}, respectively) are correlated with the load extension curve for all of the MD samples. L_{TD} results from unoriented lamellae and is therefore only present for samples O and P.

During elastic deformation, and recorded in Figure 6, there was an increase in L_{MD} in all of the samples (in Fig. 5, it is shown by the movement of the scattering peaks towards the beamstop). Figure 7 shows that the rate of increase of L_{MD} with respect to applied strain generally increased with decreasing dominant lamellar thickness.

As well as an increase in L_{MD}, the azimuthal (i.e., perpendicular to the meridian) width of the scattering peak increased steadily during elastic deformation (shown in Fig. 8). In the region of the load-extension curve, where yielding occurred,

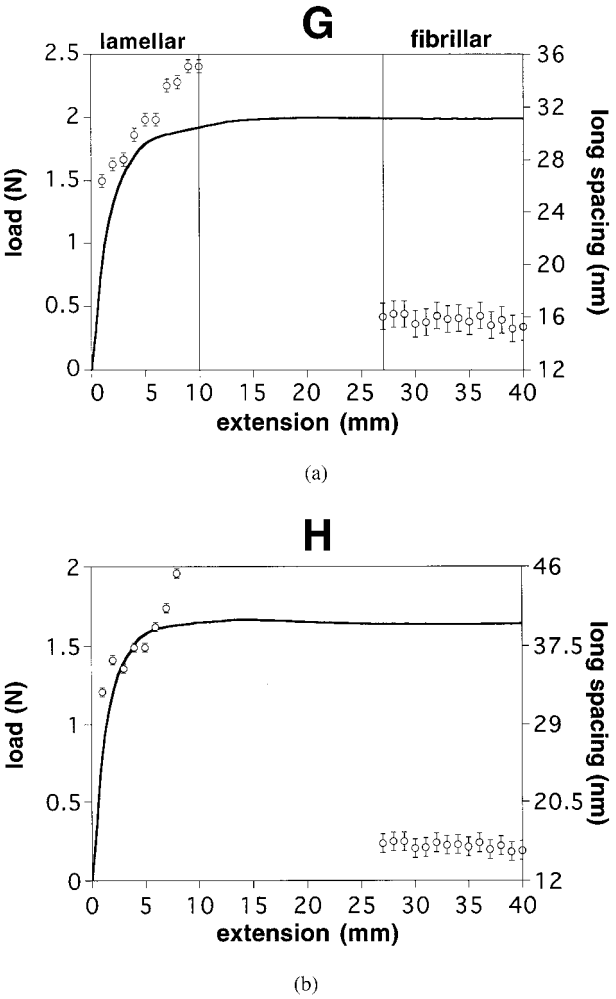

Figure 6 Correlation between the load-extension curve [L_{MD} (open circles)] and L_{TD} (filled circles) for all blown film samples drawn parallel to MD. The regions of lamellar and fibrillar scattering are indicated for sample G, as an illustrative example. (a) Sample G; (b) sample H; (c) sample N; (d) sample O; and (e) sample P.

the SAXS pattern changed markedly, and a distinct 4-point pattern emerged from the azimuthally widening 2-point pattern. The regions in Figure 6 for which no long spacing is marked correspond to the strains at which the 4-point patterns existed, and no scattering was measured on the meridian.

Figure 5 shows how the 4-point pattern remained present throughout the drawing, but became progressively weaker. It was retained to a greater extent by the hexyl- and ethyl-branched materials P and G, respectively, but had virtually disappeared by the final strain of 570% for the other samples. Accompanying the change in intensity was a change in the shape of the pattern as the "arms" forming the 4-point pattern moved to increasingly larger angles away from the tensile axis and MD.

Figure 9 illustrates the evolution of the SAXS intensity profile parallel to the tensile axis and

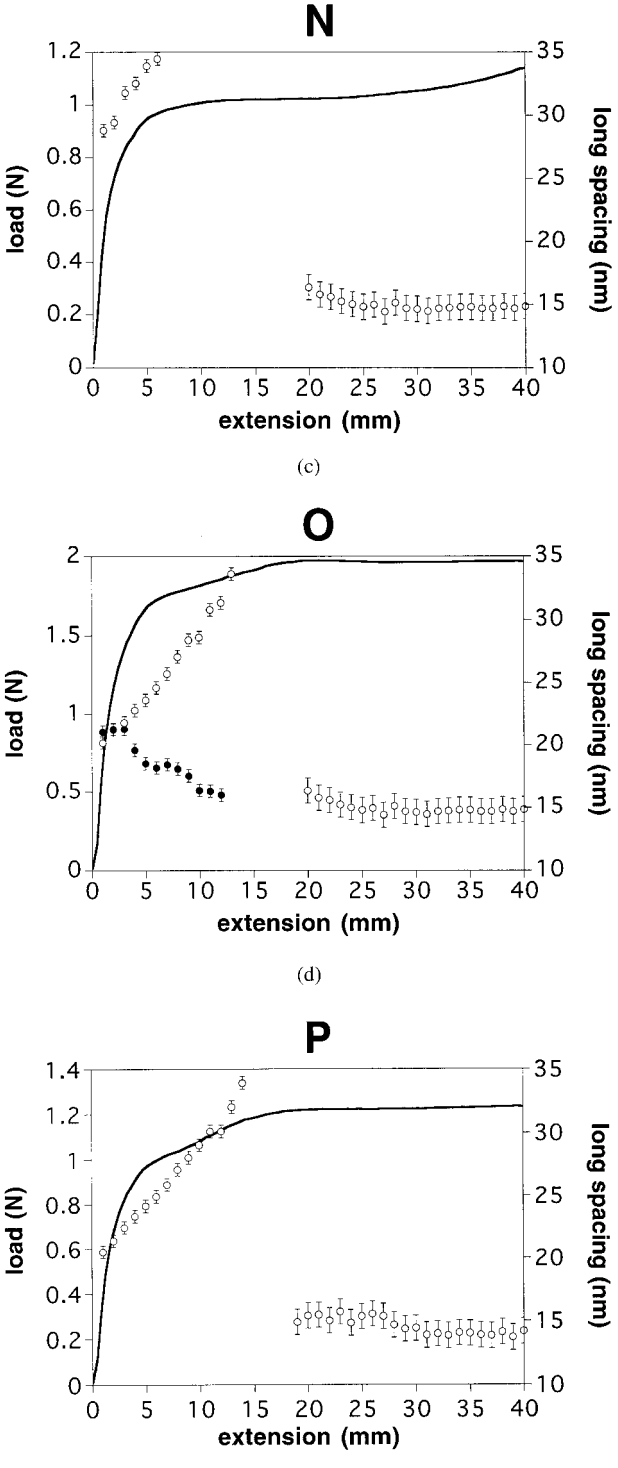

Figure 6 (*Continued*)

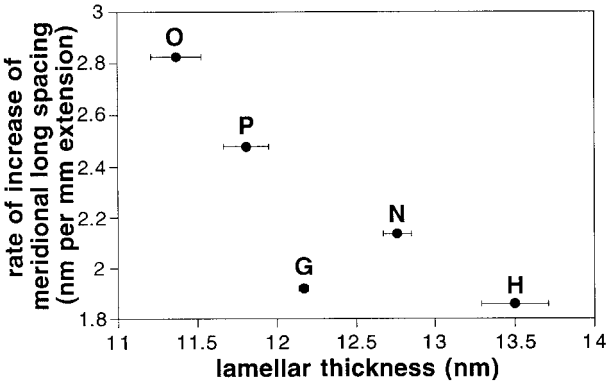

Figure 7 Variation of the rate of increase with respect to applied strain of L_{MD} for all samples (G, H, N, P, and O) drawn parallel to MD.

MD for G, H, and O, showing the gradual loss in intensity and disappearance of the initial lamellar two-point SAXS peak and its replacement with a much weaker peak (arrowed) due to scattering from a fibrillar morphology. The fiber peak, which appeared during the plateau region of the load extension curves, coexisted with the lamellar 4-point pattern. The strain at which the fibrillar morphology was definitely identified seemed unrelated to the microstructural variables or to the values of applied load. Values for the fiber long spacings of the different samples were G, 15.6 ± 0.1 nm; H, 15.7 ± 0.1 nm; 0, 14.8 ± 0.1 nm; P, 14.1 ± 0.1 nm.

Drawing Perpendicular to MD (Parallel to TD)

Figure 10 illustrates the changes in the two-dimensional SAXS pattern during drawing for sample P, which was typical of all of the samples. The load extension curve is shown in Figure 5(b). The peak width parallel to MD increased (Fig. 10), whereas azimuthally becoming narrower (shown in Fig. 11). The long spacing parallel to MD decreased from the start of deformation (shown in Fig. 12). In samples G and P, it can be seen that L_{MD} began to decrease at a slower rate near the onset of the load-extension curve plateau, although such an effect was not seen in the other samples. For sample P, for which there was also some scattering perpendicular to MD, L_{TD} increased in the same manner as L_{MD} for the samples drawn parallel to MD, and disappeared at the end of the elastic deformation region. The lamellar peak was present throughout the whole deformation range for all of the samples except for sample H, in which it rapidly disappeared with the onset of the load-extension curve plateau. The rate of decrease, with respect to applied strain, of L_{MD} seemed to be roughly correlated with lamellar thickness: the thicker the dominant lamellae, the less rapid was the decrease in L_{MD}.

During the load-extension curve plateau, a fibrillar morphology developed in sample O that resulted in a very weak peak parallel to the tensile axis. The fibrillar and lamellar morphologies coexisted. The value of the fiber long spacing in this specimen was the same as that in the specimen drawn parallel to MD and was 14.7 ± 0.1 nm. No fiber peak was identified with complete certainty in any of the other samples drawn perpendicular to MD.

In Figure 10, it can be seen that, for sample P, there was some scattering forming two diametrically opposed arcs above and to the left and below and to the right of the beamstop away from the main lobe of scattered intensity. This was also observed in the other hexyl-branched material, sample O, but not in the other samples. The long spacing measured from these arcs was the same as that of the initial undeformed material.

Drawing at 45° to MD

Drawing at 45° to MD caused an initial rotation of the 2-point pattern away from the tensile axis during elastic deformation [shown in Fig. 13, which illustrates the evolution of the SAXS pattern for sample P drawn at 45° to MD; the simultaneously obtained load-extension curve is shown in Fig. 5(b)]. Upon macroscopic yielding, the spots became flattened in the direction of the tensile axis. With further deformation, the lamellar scattering disappeared and was replaced by a new long spacing, presumably resulting from a fibrillar morphology.

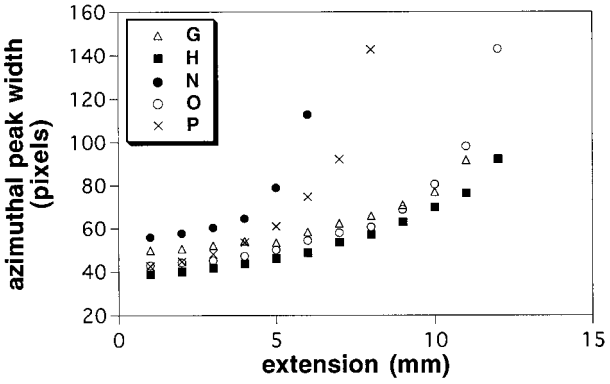

Figure 8 Increase in azimuthal peak width during drawing parallel to MD for all samples.

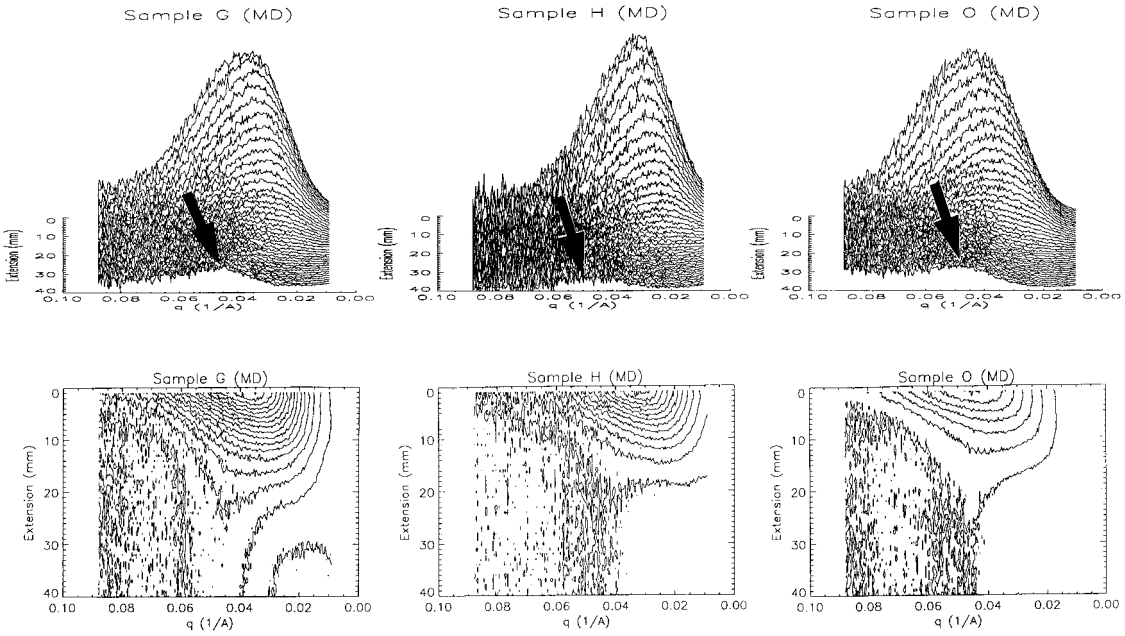

Figure 9 Evolution of the SAXS peak parallel to MD during drawing parallel to MD for G, H, and O. The top plots show the evolution of the meridional SAXS intensity profile, in which the peak due to fibrillar scattering is arrowed. Beneath are the contour plots, in which the position of the fiber peak may be identified more easily.

Time-Resolved SALS

H_v Scattering

The H_v SALS patterns from all samples were very similar. Patterns from samples drawn parallel to MD contained a lot of diffuse scattering. Upon this background were imposed four lobes of higher intensity oriented at 45° to MD (Fig. 14, frame 1). Within each lobe, the intensity decreased monotonically with increasing scattering angle, and no distinct peak was observed.

Figure 14 shows a sequence of H_v SALS patterns and the simultaneously obtained load-extension curve for sample G drawn parallel to MD. The overall integrated scattered intensity increased during elastic deformation and yield, and then decreased again at higher strains. This effect is confirmed in Figure 15, where the overall scattered intensity (i.e., integrated over the entire scattering pattern) is plotted over the load-extension curves for both samples. During deformation, the appearance of the four lobes changes, becoming flattened in the direction of the tensile axis, and four new, less intense, lobes appeared at 24% nominal strain at a larger angle to the tensile axis. These new, smaller lobes rapidly became overwhelmed by the general increase in intensity and were not visible after the intensity had begun to decrease again.

Figure 16 shows a sequence of H_v SALS patterns and the simultaneously obtained load-extension curve for sample H drawn perpendicular to MD. It can be seen that the initial shape of the scattering pattern was quite different from the SALS pattern when MD was oriented parallel to the tensile axis. There were no lobes, and the SALS pattern was virtually circular. During deformation, this pattern became elongated in the direction perpendicular to the tensile axis. Figure 17 shows that, apart from an initial period during the first stages of elastic deformation when there was little change in the scattering pattern, the circular pattern deformed affinely. The eccentricity of the pattern was measured by measuring the distance between two points of equal intensity parallel and perpendicular to the tensile axis, and is also shown in Figure 17.

Figure 18 shows a series of H_v SALS patterns and the simultaneously obtained load-extension curve for sample H drawn at 45° to MD. The initial SALS pattern was very similar to the pattern from sample H, with MD perpendicular to the tensile axis. However, during deformation, the four-lobe type pattern that was observed when MD was parallel to the tensile axis began to emerge and rotate into view. The four lobes initially became more distinct as drawing continued, although a fully symmetrical pattern was not ob-

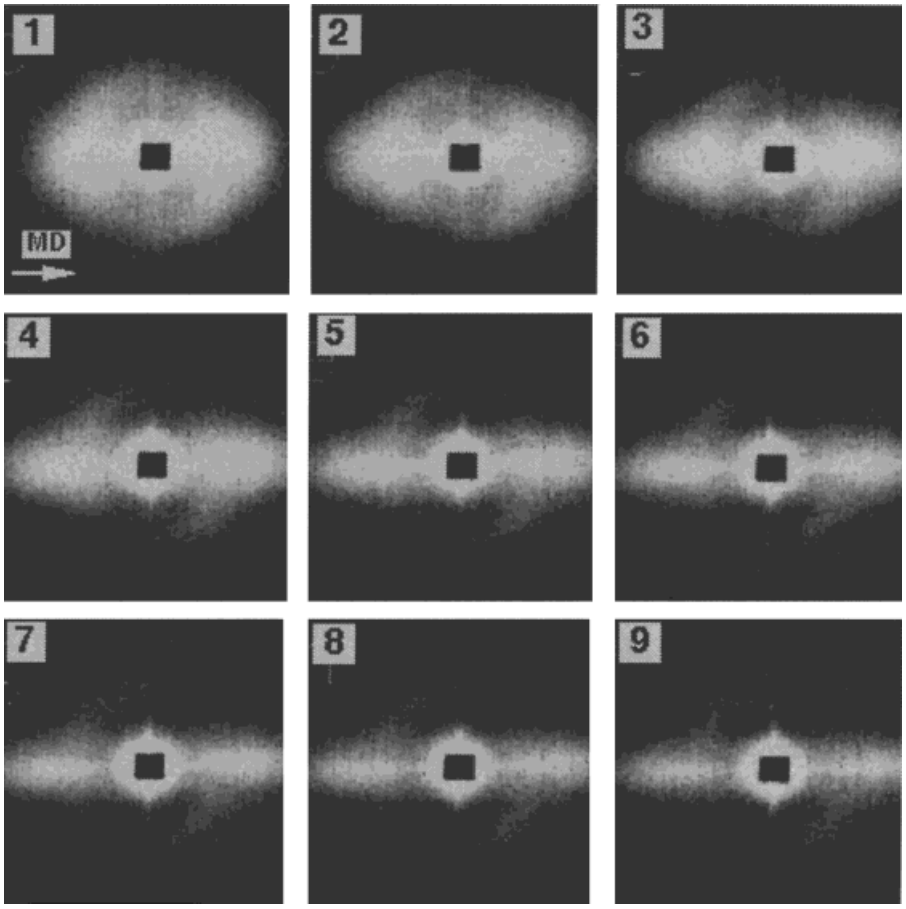

Figure 10 Sequence of SAXS patterns for sample P drawn perpendicular to MD (parallel to TD). The tensile axis is vertical. The simultaneously obtained load-extension curve is shown in Fig. 5(b), marked "TD."

tained in the attainable deformation range. At higher strains, the cross became less distinct as the lobes decreased in extent in the direction parallel to the tensile axis.

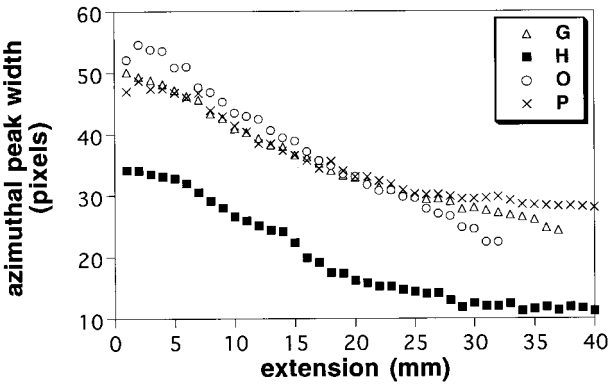

Figure 11 Reduction in azimuthal peak width (parallel to MD) during drawing perpendicular to MD (samples G, H, O, and P).

V_v Scattering

The V_v patterns for all of the undeformed samples in all three orientations (MD, TD, and 45) were initially isotropic. Figure 19 shows the simultaneously obtained V_v SALS patterns and load-extension curve for sample G drawn parallel to MD, showing the increasing ellipticity of the SALS pattern during drawing. Figure 20 shows that the eccentricity of the ellipse increased linearly with increasing strain. During elastic deformation, the overall scattering intensity (integrated over the entire scattering pattern) increased (shown in Fig. 21) before reaching a constant value at a strain of 171%.

DISCUSSION

X-ray Scattering

Lamellar Structure of the Undeformed Samples

SAXS results indicate that the samples crystallized with a stacked lamellar morphology, with

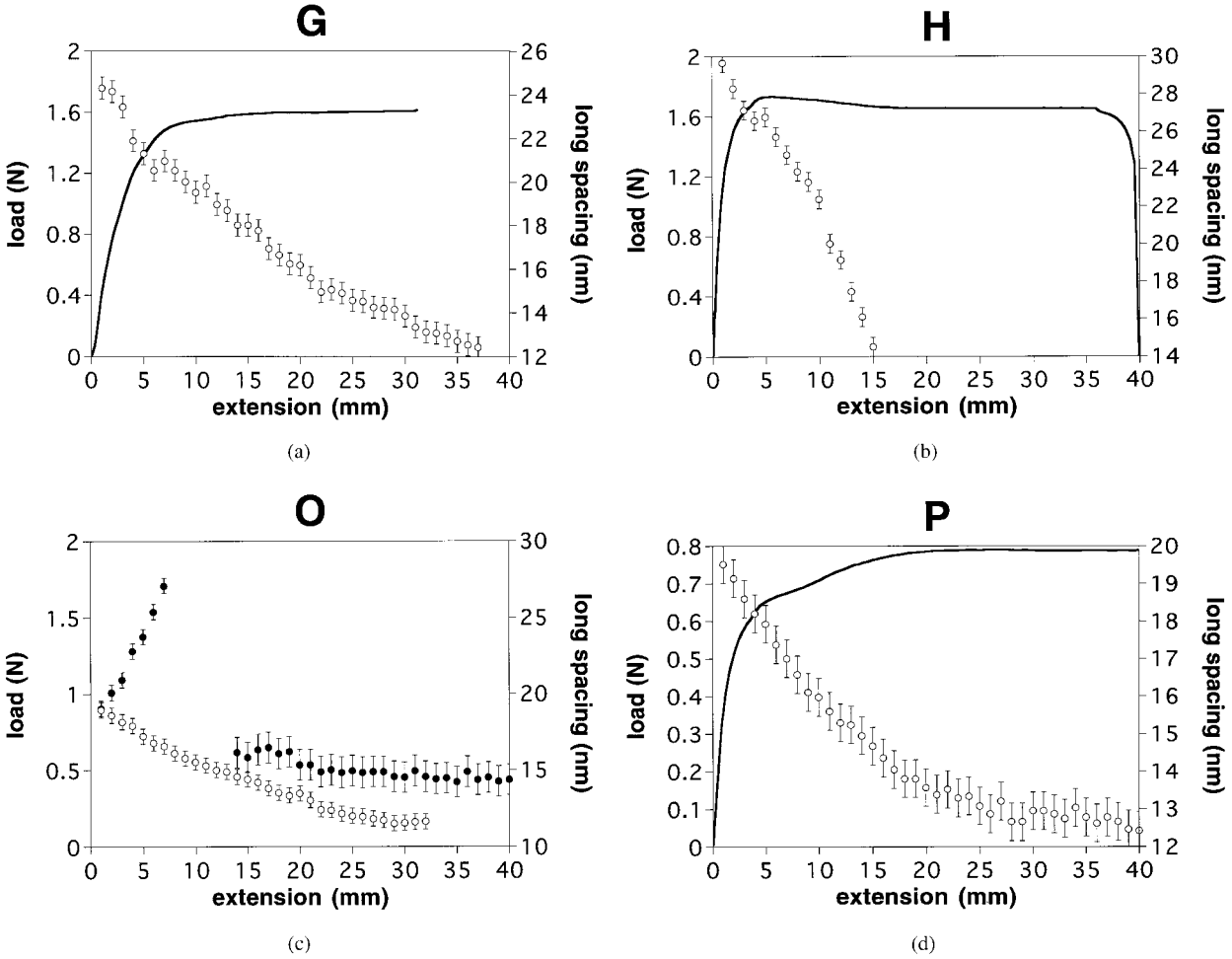

Figure 12 Correlation between the load-extension curve, L_{MD} (open circles) and L_{TD} (filled circles) for all samples except N drawn perpendicular to MD. (a) Sample G; (b) sample H; (c) sample O; and (d) sample P.

the lamellar normals oriented parallel to MD. The existence of some randomly oriented lamellar only in the less crystalline hexyl-branched materials may have been due to the sample processing history, microstructural influences (such as branch length), or the presence of a randomly oriented transcrystalline layer at the film surface. The different lamellar thickness distributions indicated by DSC provide evidence that the sample processing histories were probably different. Comparison of the behavior of the different samples is therefore limited, because the influences of the different variables cannot be separated.

Drawing Parallel to MD

Results from the sample drawn parallel to MD may be interpreted simply. During elastic deformation, the increase in L_{MD} resulted from interlamellar separation. Operation of fine chain slip during macroscopic yielding leading to lamellar corrugation explains the formation of the 4-point pattern. A transmission electron microscopic study[21] of the deformation mechanisms in bulk LLDPE found direct evidence for lamellar corrugation in the equatorial regions of spherulites where, as for the films drawn parallel to MD, the lamellar normals are parallel to the tensile axis. Another study[22] has directly related a corrugated lamellar morphology, imaged using transmission electron microscopy, with a 4-point SAXS pattern. Strong support for this argument is also provided by Gerasimov and colleagues,[31] who studied extruded low-density polyethylene (LDPE) films drawn to different strains using SAXS. Their SAXS patterns followed the same sequence of changes as the SAXS patterns presented in Fig. 5. They ascribed the 4-point pattern to the bending and corrugation of lamellae.

Gradual lamellar disruption and deformation of the lamellar structures explains the decrease in intensity and the movement of the SAXS intensity

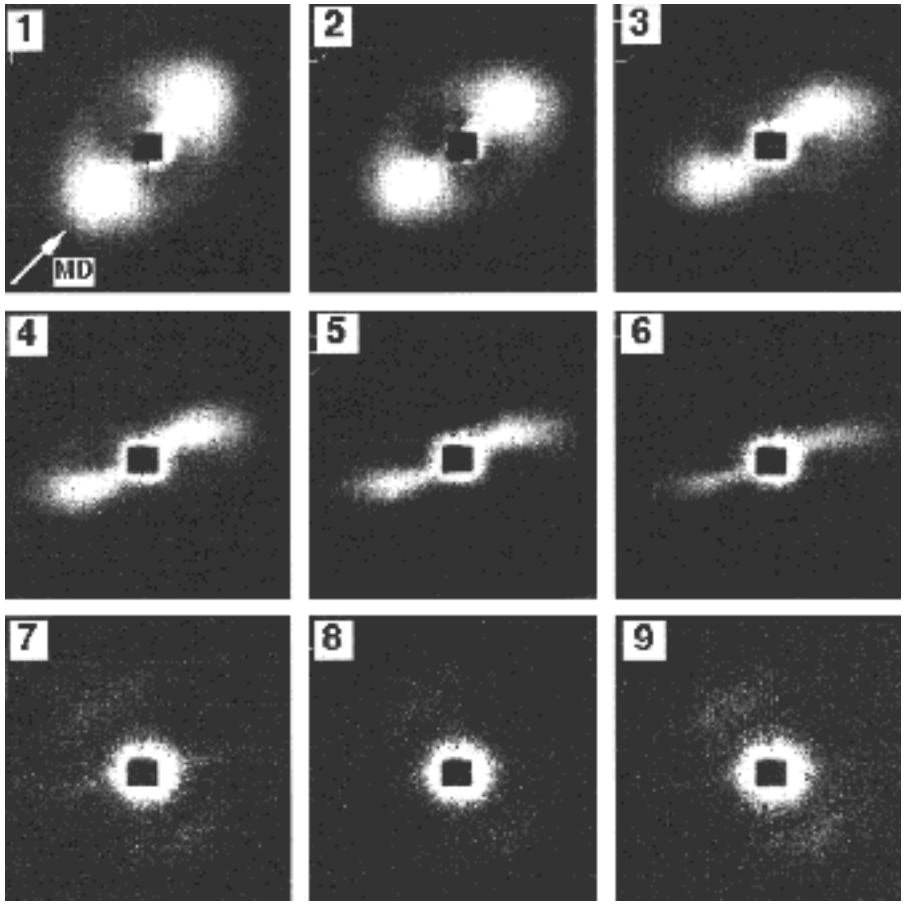

Figure 13 Sequence of SAXS patterns for sample P drawn at 45° to MD. The tensile axis is vertical. The simultaneously obtained load-extension curve is shown in Fig. 5(b), marked "45."

toward the equator as the lamellar normals rotate away from the tensile axis. It is suggested that fiber formation occurred with the advent of coarse chain slip and lamellar disintegration. A similar mechanism was proposed to occur in LDPE film by Gerasimov et al.[23] The coexistence of lamellar and fibrillar morphologies demonstrates the continuous nature of the lamellar to fibrillar transition in the LLDPE blown films studied herein. Evidence for a greater amount of crystallographic deformation in the more crystalline samples was provided by the observation that the lamellar scattering had disappeared by the highest strain for the most crystalline sample H, but was still strongly present in the least crystalline samples (O and P).

Similar values of the fiber long spacings for the different films are expected from similar values of the initial lamellar thicknesses. However, the observation that the thicker the lamellae the larger the fiber long spacing shows that the fibrillar morphology was related to the initial lamellar one. This supports the hypothesis that the lamellar to fibrillar transition occurs by purely mechanical means at room temperature, because in the melting and recrystallization scenario, the fiber long spacing is independent of initial morphology, being governed only by the sample temperature.

Drawing Perpendicular to MD (Parallel to TD)

The retention of scattering parallel to MD (i.e., perpendicular to the tensile axis) when the films were drawn perpendicular to MD shows that the lamellae did not corrugate in this direction, but slid past each other by interlamellar shear. The reduction in azimuthal width of the lamellar scattering peak suggests that the lamellar normals became more perfectly aligned perpendicular to the tensile axis and/or the lateral dimension of the lamellae increased. Whereas the former suggestion is a most likely process, a mechanism for the latter remains uncertain. Possibly, lamellae slide into place next to each other to form larger lamellae with a greater lateral extent.

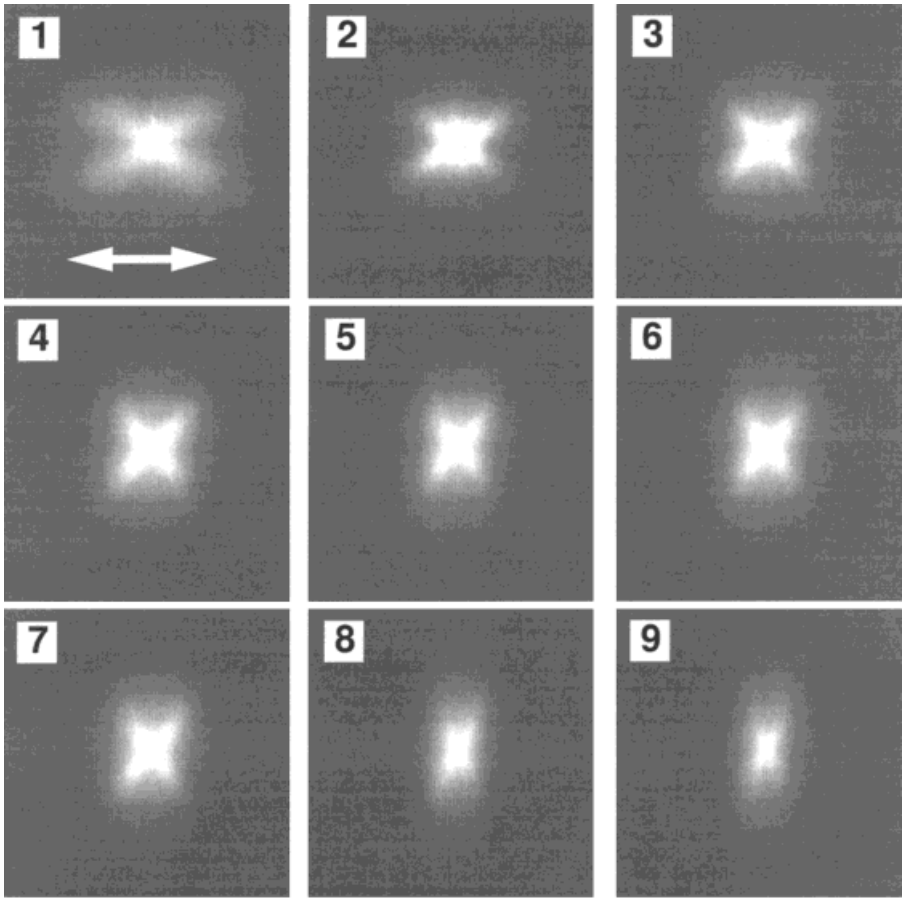

(a)

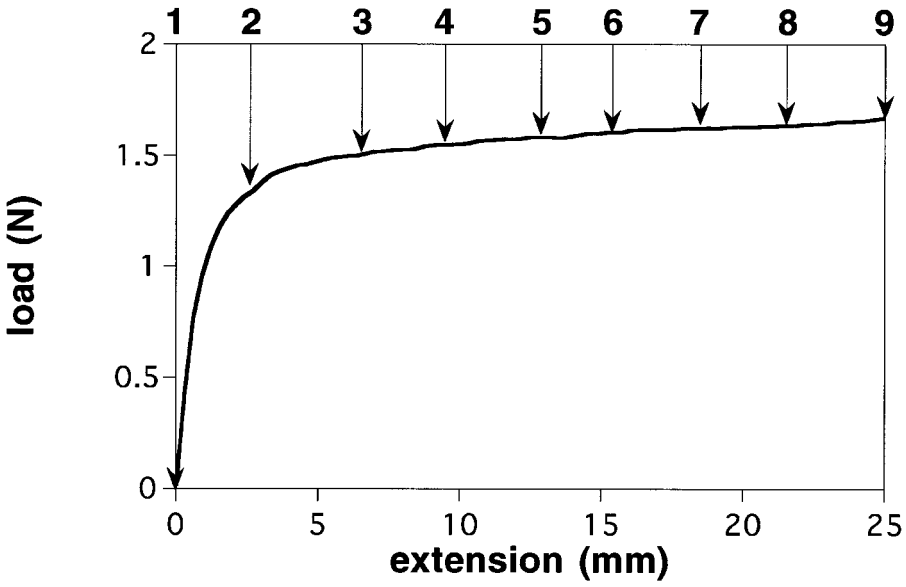

(b)

Figure 14 (a) Sequence of H_v SALS patterns and (b) the simultaneously obtained load-extension curve for sample G drawn parallel to MD. The tensile axis and MD are arrowed in frame 1.

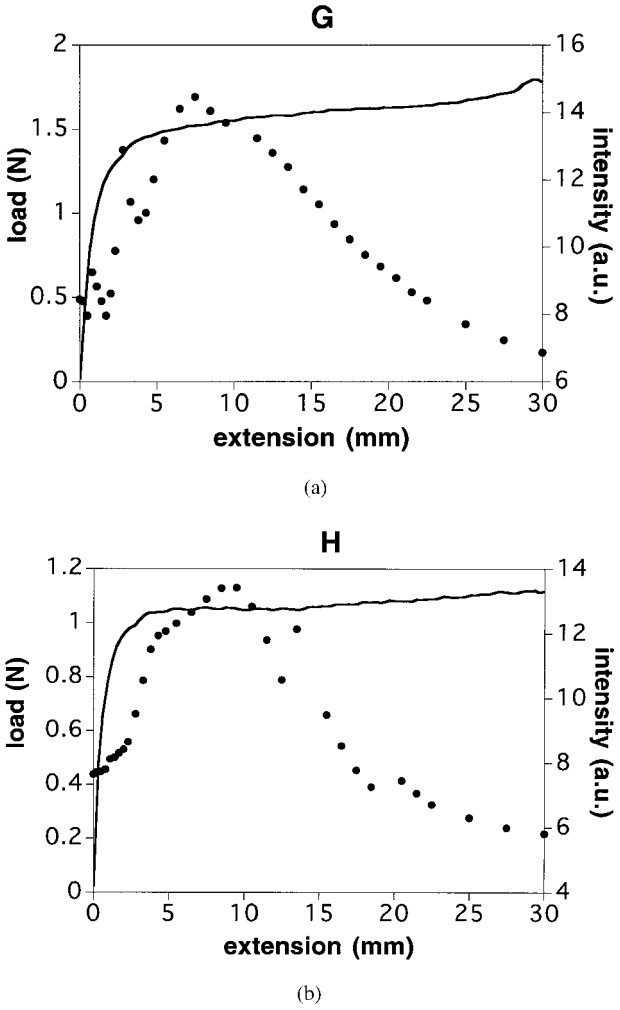

Figure 15 Correlation between the H_v SALS intensity (points) and the load-extension curve (continuous line) for (a) sample G and (b) sample H drawn parallel to MD.

The reduction in L_{MD} during drawing may be explained by lamellar thinning caused by chain slip. However, the decrease in L_{MD} throughout both elastic and plastic deformation indicates the possibility of the operation of simultaneous shear and rotation, as described previously.[16] Insufficient information is available to differentiate between lamellar thinning caused by chain slip and a reduction in long spacing caused by shear and rotation. It is therefore impossible to relate macroscopic yielding with the onset of chain slip, as was possible in bulk copolymer samples.[17]

Eventual disintegration of the lamellae yields the fibrillar morphology. The mechanism of the lamellar to fibrillar transformation was the same as in the films drawn parallel to MD, because the fiber long spacing was the same in films drawn both parallel and perpendicular to MD.

Drawing at 45° to MD

Lamellar rotation was shown to operate during elastic deformation, because the scattering pattern rotated without change of shape. However, the subsequent development of asymmetry indicated that intralamellar shear, by chain slip, was activated in the region of macroscopic yield and resulted in eventual alignment of the molecules with the tensile axis (shown by WAXS). Continued lamellar stack rotation would have led to the opposite orientation of the chains.

Relation of Oriented PE Deformation to Spherulite Deformation

Figure 22 shows the SAXS patterns at three extensions from samples drawn parallel, perpendicular, and at 45° to MD (1st, 2nd, and 3rd rows respectively). The 4th row is composed of the addition of the first three rows. The composite pattern thus obtained is qualitatively similar to the patterns obtained at different strains from a bulk, initially unoriented, specimen of the same PE grade.[17] Therefore, it is concluded that the mechanical behavior of different regions of a spherulite may be modeled to a first approximation by the behavior of oriented samples. It is worth mentioning that a similar conclusion was drawn by Gerasimov et al.,[23] who compared the results of LLDPE films drawn parallel and perpendicular to MD with those from initially unoriented bulk LLDPE samples. Figure 23 summarizes the operative deformation modes in different regions of PE spherulites, as indicated by the results from the deformation of thin films.

SALS

H_v Scattering

Light scattering results from polymer films are in many ways more difficult to interpret than those from X-ray investigations. Because surface defects are often of a similar size to the wavelength of light, scattering may result from both structural features in the film interior and the film surfaces.[10,11] H_v scattering from polymer films has been widely studied, both experimentally and theoretically,[9,24–28] and the origin of the four-lobed pattern observed for the samples drawn parallel to MD has been interpreted in terms of scattering from structures in the film interior.[24,25,27] In blown films, these structures are found to be elliptical, with the long axis parallel to MD.[9] It has been suggested that they correspond to unfolded-chain crystals with their chain axes parallel to MD.[9]

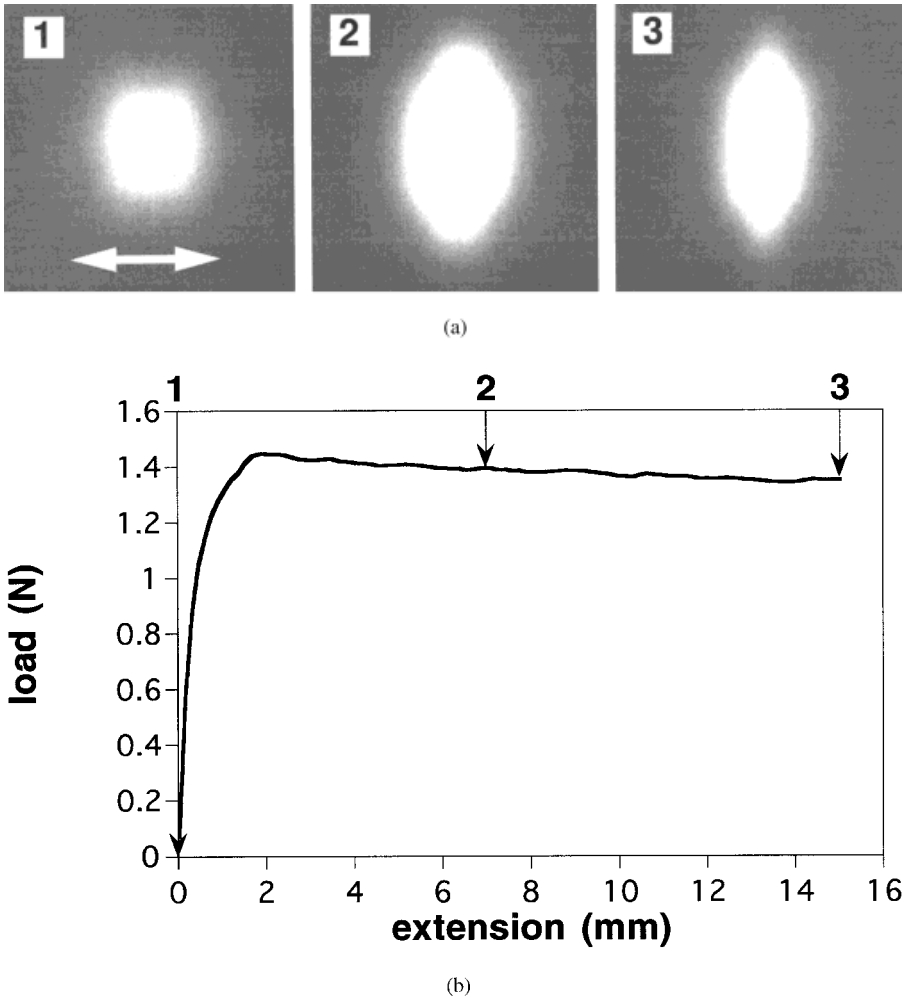

Figure 16 (a) Sequence of H_v SALS patterns and (b) the simultaneously obtained load-extension curve for sample H drawn perpendicular to MD. The tensile axis is arrowed in frame 1.

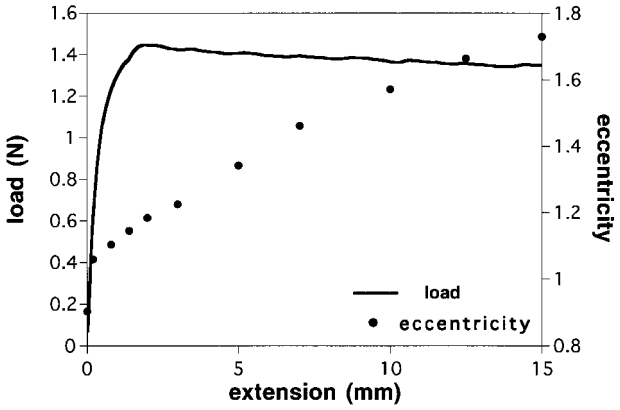

Figure 17 Correlation between the eccentricity of the H_v SALS pattern for sample H drawn perpendicular to MD and the load-extension curve.

However, SAXS provided no evidence for such crystals, but showed the presence of oriented lamellae. Therefore, it is likely that the microstructures giving rise to the four lobes in the H_v scattering from the films studied were regions of similarly oriented, or commonly nucleated, lamellae. The diffuse isotropic scattering was probably due to surface roughness.[10,11] Indeed, it is known that the majority of the light scattering from LLDPE films results from surface roughness, because coating the film with oil of equal refractive index reduces the light scattering to markedly lower levels.[10]

The H_v scattering from the samples drawn parallel to MD resembled those obtained in studies of PE spherulite and polypropylene (PP) blown film deformation[24,25] that also yielded a four-lobed pattern in which the extent of the lobes in the direction parallel to the tensile axis decreased during drawing. The four-lobed pattern has been

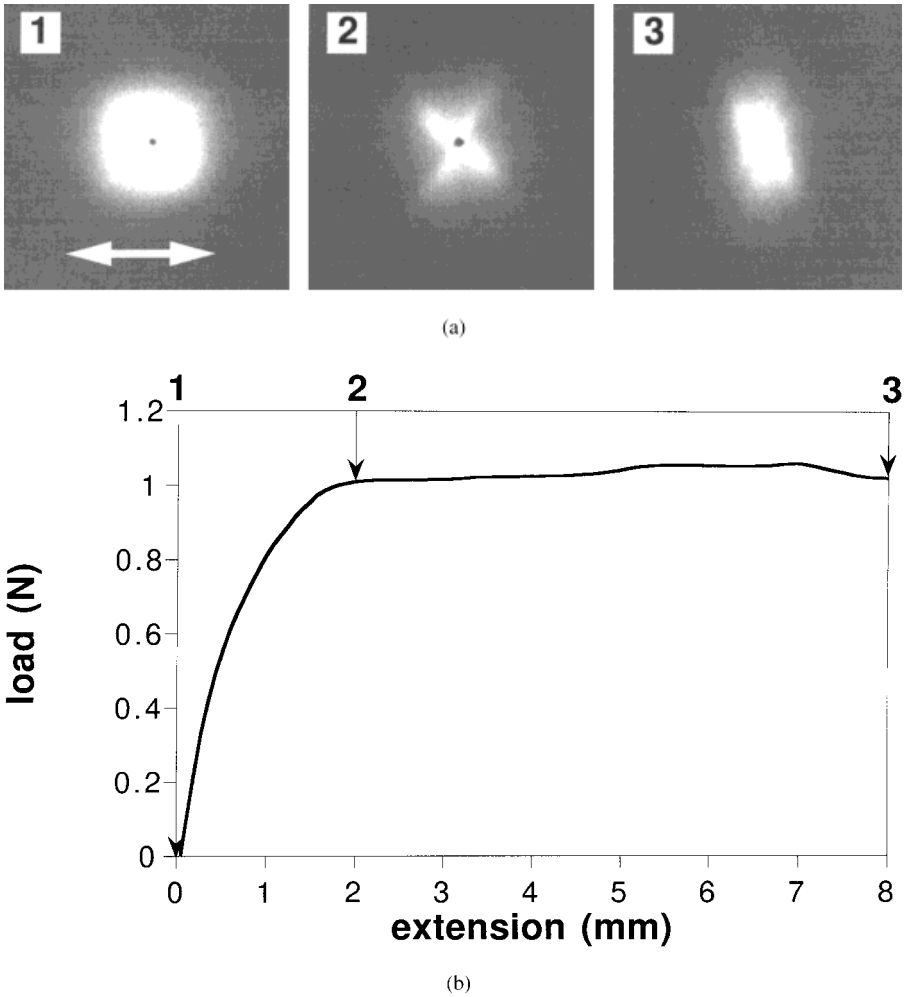

Figure 18 (a) Sequence of H_v SALS patterns (b) and the simultaneously obtained load-extension curve for sample H drawn at 45° to MD. The tensile axis is arrowed in frame 1.

associated with a sheaf-like morphology in which the sheaves were aligned side by side with their axes perpendicular to MD, and has been found in LLDPE and polybutene-1 blown films.[24] The SAXS results suggest that, in this case, the sheaves consist of similarly oriented lamellae. Deformation of the sheaves caused them to elongate in the drawing direction as the lamellae separated, which explains the reduction in extent of the light scattering in this direction during drawing.

The presence of four smaller lobes at a larger angle to MD than the main lobes has been previously noted in both deformed and undeformed oriented films.[24] In undeformed polybutene-1 blown film, the small lobes have been attributed to interference from assemblies of sheaves and seem to depend on the orientation of the sheaves within the film. A similar explanation may be used in the case of the LLDPE films studied herein. SAXS has shown that lamellae, and hence sheaves, oriented with their normals at an angle to the tensile axis rotate away from it during drawing. The increase in azimuthal width of the SAXS peak apparent during elastic deformation for the samples with lamellar normals parallel to the tensile axis signifies a decrease in lamellar orientation. The appearance of the new SALS lobes during elastic deformation therefore suggests the possibility that drawing causes changes in orientation that enable the new lobes to appear.

The causes of the changes in H_v SALS pattern for the sample drawn perpendicular to MD are harder to ascertain. Two regions of behavior are apparent: (1) the initial stages of elastic deformation in which the SALS pattern changes shape most rapidly; and (2) this stage, which lasts for the remainder of the deformation, in which the

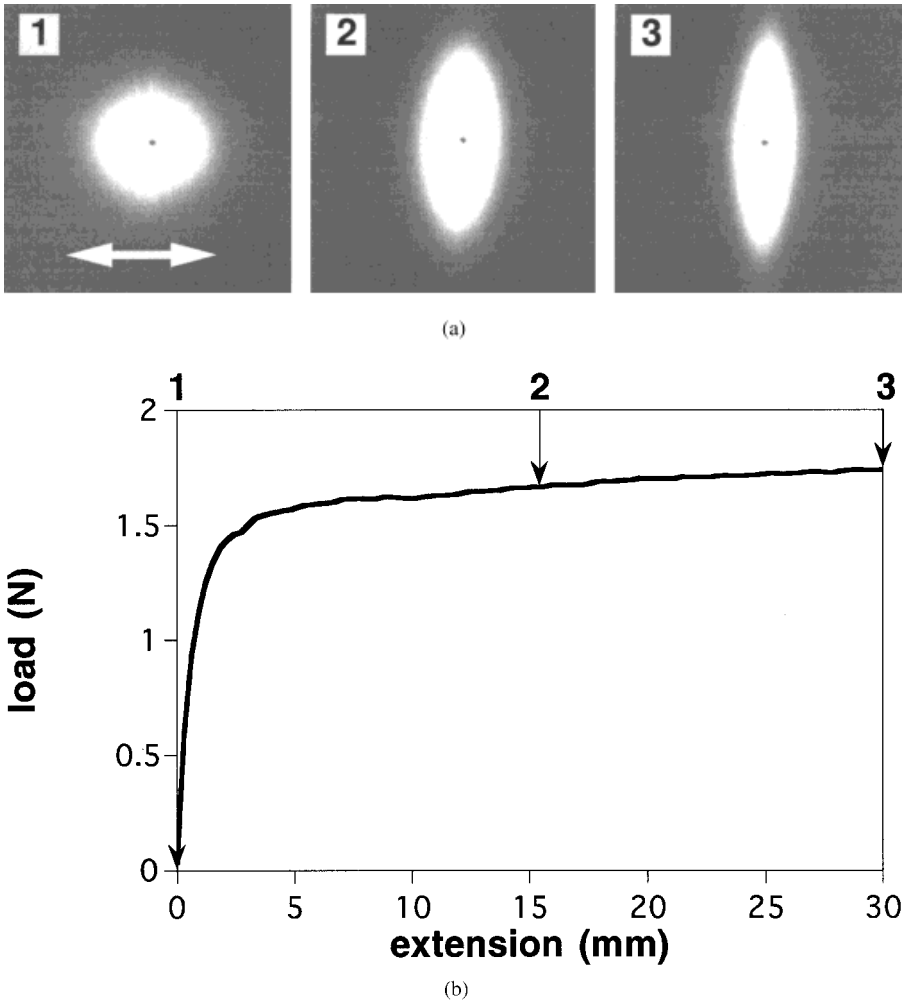

Figure 19 (a) Sequence of V_v SALS patterns and (b) the simultaneously obtained load-extension curve for sample G drawn parallel to MD. The tensile axis and MD are indicated in frame 1.

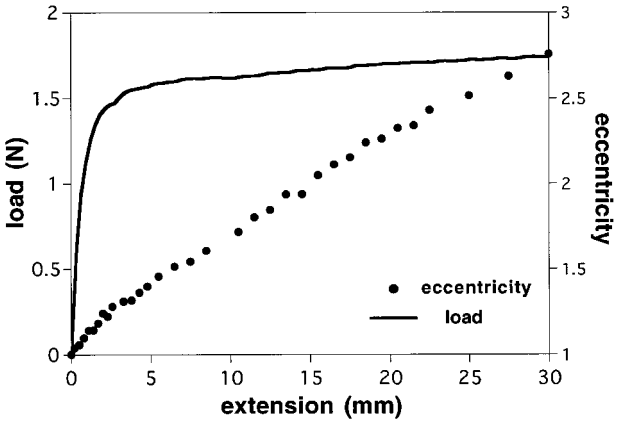

Figure 20 Correlation between the eccentricity of the V_v SALS pattern of sample G drawn parallel to MD and the load-extension curve.

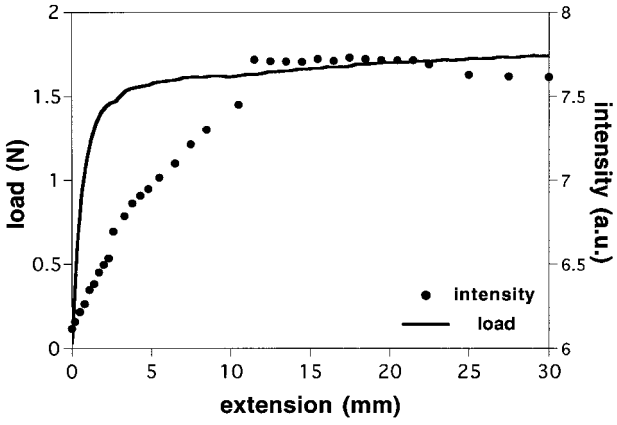

Figure 21 Relationship between the V_v SALS intensity and the load-extension curve for sample drawn parallel to MD.

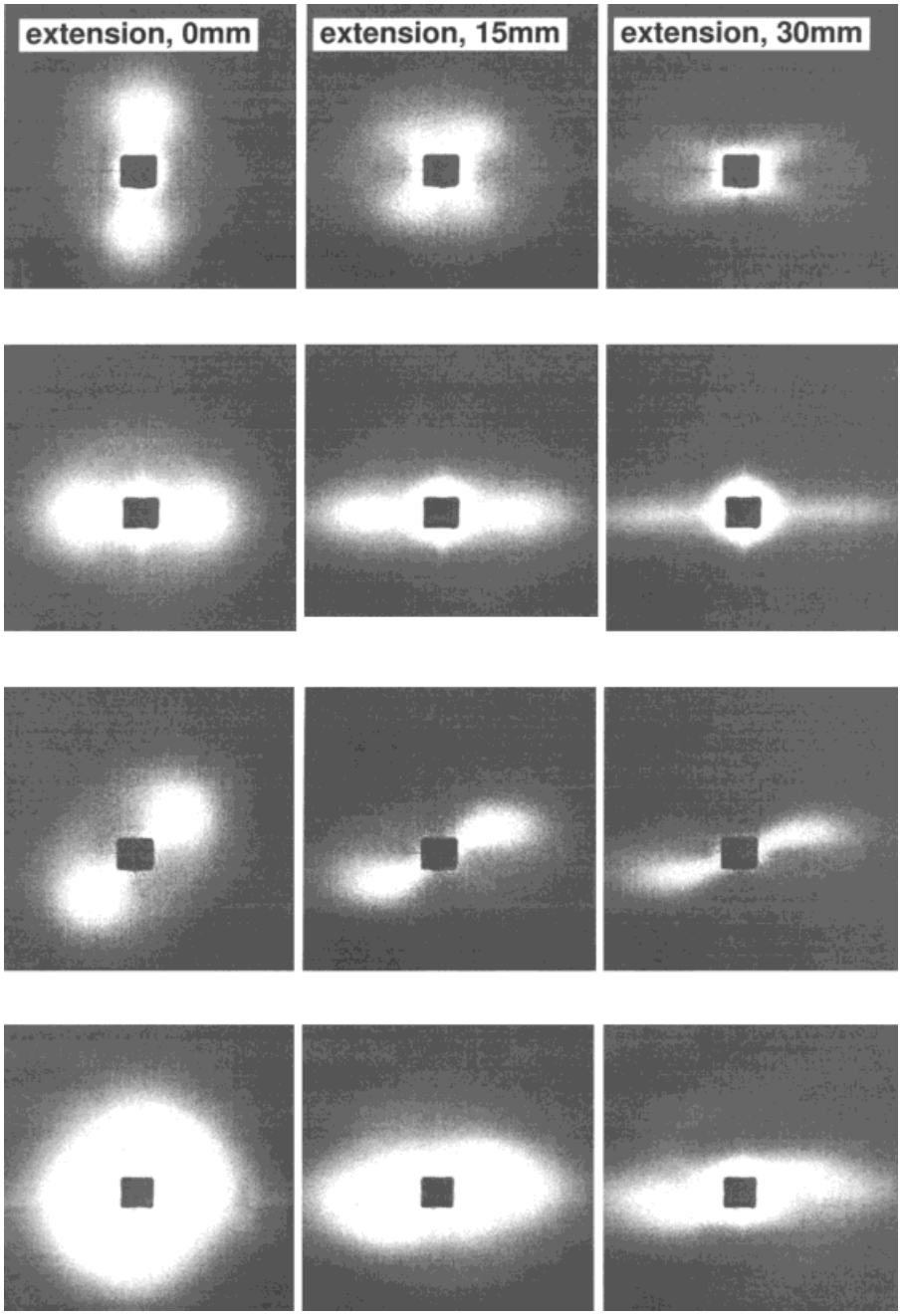

Figure 22 Construction (bottom row) of SAXS patterns from deformed spherulites by superimposing the patterns from an oriented sample deformed parallel to MD (1st row), perpendicular to MD (2nd row), and at 45° to MD (3rd row).

SALS pattern changes shape at a constant rate. Unlike the case of deformation parallel to MD, the effects of deformation perpendicular to MD are not well documented. It is therefore impossible at this stage to separate the influences of internal and surface structure on the SALS pattern, and further analysis is not attempted.

The H_v SALS pattern from the sample drawn at 45° to MD provides evidence for lamellar rotation, but apparently in the opposite direction to that observed by SAXS. The appearance of four lobes out of an initially isotropic scattering pattern, and their subsequent rotation during further drawing, could be interpreted as the rotation of lamellar bundles from a position where their axes were oriented at 45° to the tensile axis to one approaching 90° to the tensile axis. SAXS, however, showed that the rotation occurred in the op-

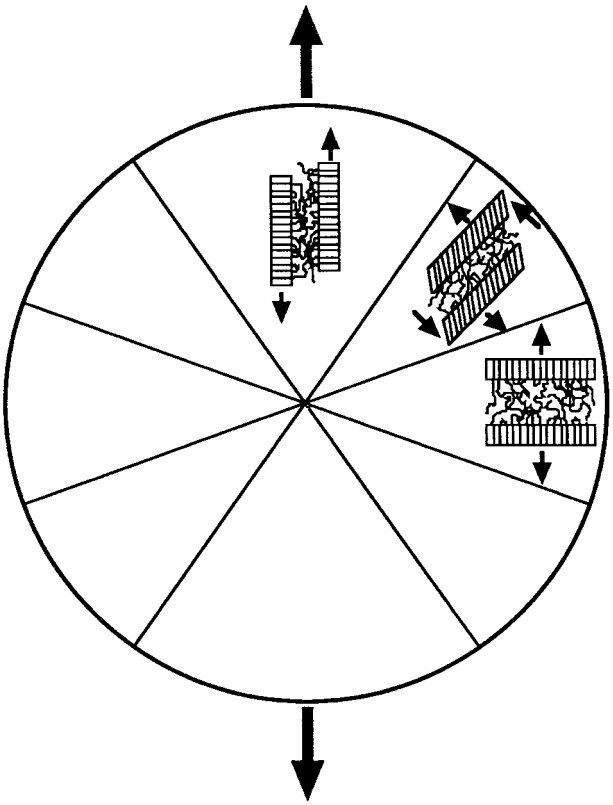

Figure 23 Schematic illustration of lamellar deformation modes operative in different regions of spherulitic samples.

posite sense. To account for this discrepancy, it is suggested that molecular, as well as lamellar, orientation within the lamellar bundles must also be accounted for.

Finally, a number of factors contribute to the overall scattered intensity. The initial increase in scattered intensity measured when the samples were drawn parallel to MD may have been due to sample thinning reducing beam attenuation, as well as a greater scattered intensity from the film interior. However, if beam attenuation was important, the decrease in intensity at higher strains would not have occurred. This decrease may have resulted from a reduction in scattering from surface roughness as the samples became smoother during drawing.

V_v Scattering

Two mechanisms have been proposed to account for surface roughness, which is found to be a major contributor to the V_v scattering from blown films[10,11]: bumps and irregularities formed in the extrusion process and crystalline aggregates formed at, or near, the film surface. Of these, the former is the predominant mechanism contributing to the V_v scattering from blown films.[10,11]

With this interpretation, the evolution of the V_v SALS patterns may be interpreted straightforwardly. Initially, the surface bumps and irregularities must be randomly distributed and fairly circular for the isotropic scattering to arise. During deformation, the bumps become elongated in the draw direction and become elliptical in shape, resulting in the increase in equatorial SALS. Affine deformation of the bumps results in the linear increase in ellipticity of the V_v SALS pattern during drawing. The increase in intensity measured by the detector probably results from a reduced attenuation of the light beam as the sample thinned during deformation.

CONCLUSIONS

A range of LLDPE blown films were studied. SAXS showed that they possessed oriented lamellar morphologies, with the lamellar normals parallel to MD, and SALS indicated that the lamellae bundled together in sheaf-like structures. A certain amount of unoriented lamellae was detected in materials containing hexyl branches, although no conclusive evidence was found for its cause. WAXS suggested that a Keller/Machin I morphology was adopted (i.e., that the lamellae were twisted) and that there was slight overall orientation of the molecules parallel to MD in the amorphous component.

The initial lamellar orientation determined the operative deformation mechanisms during elastic deformation. Interlamellar separation occurred when the lamellae were perpendicular to the tensile axis, interlamellar shear when they were parallel to the tensile axis, and lamellar stack rotation when they were inclined at 45° to the tensile axis. Macroscopic yielding was caused by the activation of chain slip, which led to lamellar corrugation in the first case, lamellar thinning in the second, and intralamellar shear in the third. It is proposed that the deformation mechanisms described in the previous three cases, during both elastic deformation and yielding, describe the deformation mechanisms that operate in the equatorial, polar, and inclined regions of spherulites, and can be used to explain the microstructural changes observed during the deformation of unoriented samples. In all cases, lamellar fragmentation ultimately occurred, over a range of strains, and led to the formation of a fibrillar morphology. The dependence of the fiber long spacing on the

initial lamellar microstructure provided evidence that, at room temperature, yielding occurred by mechanical deformation only.

At larger length scales, light scattering (especially in the V_v configuration) from the samples was dominated by scattering from surface roughness, and the evolution of the SALS patterns during drawing mainly reflected the elongation of surface irregularities. Some scattering was interpreted as arising from the internal structure; however, in the H_v configuration. It was interpreted as scattering from sheaf-like lamellar bundles and showed the elongation of the bundles parallel to the tensile axis as the lamellae separated during drawing. It is concluded that a more comprehensive investigation is necessary, however, in which the films are coated with a refractive index-matched oil, to eliminate surface roughness scattering and provide more interesting data on the evolution of the internal microstructure during deformation.

The help of the following people is gratefully acknowledged: Dr. Elinor Kerr and Dr. Warren Reed of BP Chemicals Ltd., Mary Vickers and Mary Heppenstall-Butler of the University of Cambridge, and Kate Burr and Dr. Anthony Ryan of University of Manchester Institute of Science and Technology (UMIST). Dr. Stuart Clarke, of the University of Cambridge, is thanked for his help with the light scattering experiments. We are indebted to Elizabeth Towns-Andrews and Dr. Geoffrey Mant for their technical support and for the provision of programs from the CCP13 software suite that were used in the data analysis. The financial support of the EPSRC and BP Chemicals is acknowledged.

REFERENCES

1. C. R. Desper, *J. Appl. Polym. Sci.,* **13,** 169 (1969).
2. W. F. Maddams and J. E. Preedy, *J. Appl. Polym. Sci.,* **22,** 2721 (1978).
3. W. F. Maddams and J. E. Preedy, *J. Appl. Polym. Sci.,* **22,** 2739 (1978).
4. E. Walenta, A. Janke, D. Hofman, D. Fanter, and D. Geiss, *Acta Polym.,* **37,** 557 (1986).
5. D. Hofman, D. Geiss, and A. Janke, *J. Appl. Polym. Sci.,* **39,** 1595 (1990).
6. R. J. Pazur, A. Ajji, and R. E. Prud'homme, *Polymer,* **34,** 4004 (1993).
7. R. J. Pazur and R. E. Prud'homme, *Macromolecules,* **29,** 119 (1996).
8. A. Gupta, D. M. Simpson, and I. R. Harrison, *J. Appl. Polym. Sci.,* **50,** 2085 (1993).
9. R. S. Stein and T. Hotta, *J. Appl. Phys.,* **35,** 2237 (1964).
10. F. Stehling, C. S. Speed, and L. Westerman, *Macromolecules,* **14,** 698 (1981).
11. A. Larena and G. Pinto, *Polym. Eng. Sci.,* **33,** 742 (1993).
12. E. S. Sherman, *Polym. Eng. Sci.,* **24,** 895 (1984).
13. D. M. Kalyon and F. H. Moy, *Polym. Eng. Sci.,* **28,** 1551 (1988).
14. D. C. Bassett, *Principles of Polymer Morphology,* CUP, London, 1981.
15. A. Keller and M. J. Machin, *J. Macromol. Sci.,* **B1,** 41 (1967).
16. M. F. Butler, A. M. Donald, W. Bras, G. E. Derbyshire, G. R. Mant, and A. J. Ryan, *Macromolecules,* **28,** 6383 (1995).
17. M. F. Butler, A. M. Donald, and A. J. Ryan, *Polymer,* **38,** 5251 (1997).
18. N. Bliss, J. Bordas, B. D. Fell, N. W. Harris, J. I. Helsby, G. R. Mant, W. Smith, and E. Towns-Andrews, *Rev. Sci. Instrum.,* **66,** 1311 (1995).
19. R. L. Bilsborrow, N. Bliss, J. Bordas, R. J. Cernik, G. F. Clark, S. M. Clark, S. P. Collins, B. R. Dobson, B. D. Fell, A. F. Grant, N. W. Harris, W. Smith, and E. Towns-Andrews, *Rev. Sci. Instrum.,* **66,** 1633 (1995).
20. S. M. Clarke, R. H. Ottewill, and A. R. Rennie, *Adv. Coll. Interface Sci.,* **60,** 95 (1995).
21. M. Furata and K. Kojima, *J. Macromol. Sci.-Phys.,* **B25,** 349 (1986).
22. G. Blöchl and A. J. Owen, *Colloid Polym. Sci.,* **262,** 793 (1984).
23. V. I. Gerasimov, Ya V. Genin, and D. Ya Tsvankin, *J. Polym. Sci., Polym. Phys. Edn.,* **12,** 2035 (1974).
24. J. M. Haudin, *Optical Properties of Polymers,* Elsevier, New York, 1986.
25. R. S. Stein and M. B. Rhodes, *J. Appl. Phys.,* **31,** 1873 (1960).
26. R. S. Stein, P. R. Wilson, and S. N. Stidham, *J. Appl. Phys.,* **34,** 46 (1963).
27. S. Clough, J. J. van Aartsen, and R. S. Stein, *J. Appl. Phys.,* **36,** 3072 (1965).
28. M. Hashimoto, A. Toda, and H. Miyaji, *Polymer,* **33,** 909 (1992).